Mechanical Systems and Signal Processing 165 (2022) 108392

Contents lists available at ScienceDirect

Mechanical Systems and Signal Processing

journal homepage: www.elsevier.com/locate/ymssp

Reconfigurable waveguides defined by selective fluid filling in two-dimensional phononic metaplates

Ting-Ting Wang [a], Yan-Feng Wang [b,*], Zi-Chen Deng [a], Vincent Laude [c,*], Yue-Sheng Wang [b,d]

[a] School of Mechanics, Civil Engineering and Architecture, Northwestern Polytechnical University, 710072 Xi'an, China
[b] School of Mechanical Engineering, Tianjin University, 300350 Tianjin, China
[c] Institut FEMTO-ST, CNRS UMR 6174, Université de Bourgogne Franche-Comté, F-25030 Besançon, France
[d] Institute of Engineering Mechanics, Beijing Jiaotong University, 100044 Beijing, China

ARTICLE INFO

Communicated by W. Ostachowicz

Keywords:
Phononic crystal
Acoustoelastic coupling
Reconfigurable waveguide

ABSTRACT

We investigate two-dimensional phononic metaplates consisting of a periodic array of cups on a thin epoxy plate that is perforated with periodic cross holes. The cups are individually filled with water or remain empty, in view of creating reconfigurable phononic waveguides. Phononic band gaps exist for empty or filled epoxy cups, leading to waveguides defined with either positive or negative contrast. Straight and 90° bent waveguides are considered experimentally. Lamb waves are excited by a piezoelectric patch glued onto the metaplate and are imaged using a scanning laser vibrometer. Experimental results are compared to a three-dimensional finite element model of fluid–structure interaction. Passing and forbidden frequency ranges are identified for positive and negative contrast, and confined propagation is observed along the waveguides. Significantly, the propagation of acoustoelastic waves in the 90° bent waveguides is observed experimentally. Reconfigurability and reusability are thus realized based on the coupling of elastic waves in the solid and acoustic waves in the fluid. The results show plenty of potentiality for the practical design of multiplexed and programmable acoustic devices implemented with reconfigurable waveguides printed on demand in a phononic metaplate.

1. Introduction

Phononic crystals (PCs) are periodic structures [1] that are engineered to manipulate the propagation of acoustic or elastic waves [2]. A significant feature of PCs is the existence of bandgaps, or frequency ranges within which wave propagation is fully forbidden due to periodicity. It is well known that many parameters influence bandgaps, such as material properties [3,4], viscosity [5–9], multifield couplings [10–13], geometric variations [14,15], or interface conditions between different components [16]. Based on these ingredients, many researchers have considered the manipulation of elastic waves in PCs [17–19]. Defect states appear inside bandgaps when periodicity is broken [20]. Various defects can be formed by changing the shape, the size, the material properties of the scatterer or of the matrix, by removing or adding scatterers, etc. Active operation can be achieved through the application of an external electrical field [21], of an external magnetic field [22,23], or of an external force [22,24]. Line waveguides and more arbitrary phononic circuits are thus formed to channel waves at selected frequencies in the bandgap with strong confinement [18,25], promising a variety of potential applications [26–28] such as sensing [29–34], filtering [35], or waveguiding [36,37].

* Corresponding authors.
E-mail addresses: wangyanfeng@tju.edu.cn (Y.-F. Wang), vincent.laude@femto-st.fr (V. Laude).

https://doi.org/10.1016/j.ymssp.2021.108392
Received 27 May 2021; Received in revised form 23 July 2021; Accepted 22 August 2021
Available online 2 September 2021
0888-3270/

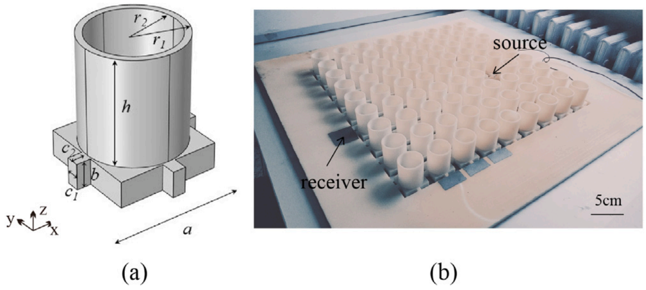

Fig. 1. The reconfigurable phononic metaplate considered in this work is based on the periodic unit cell depicted in (a). The 3D-printed epoxy metaplate sample (b) contains 9 × 8 periodic unit cells. One cup is removed inside the phononic structure to bond a piezoelectric patch for excitation of Lamb waves. Imaging of wave propagation is performed on the bottom side of the plate.

To date, many works have focused on Lamb wave guiding. Wang et al. investigated experimentally Lamb wave propagation in coupled-resonator elastic waveguides formed by a chain of cavities in a two-dimensional steel PC slab with cross holes [37]. A straight waveguide and a wave splitting circuit with 90° bends were realized and strongly confined guiding and splitting at waveguide junctions were observed. Ghasemi Baboly et al. [38] designed and fabricated an isolated, single-mode, 90° bent PC waveguide by not drilling certain circular air holes in an aluminum substrate. Zhu et al. designed orthogonal linear waveguides coupled by a defect cavity [35]. Whatever the quality of the design, however, the manipulation of waves remains hardly reconfigurable once such a solid-state device has been manufactured. Thus, it is desirable to control waves flexibly, actively, or smartly. In recent years, there have been an increasing number of researches on tunable [39] or active manipulation of waves, either by mechanical means or basing on multifield coupling effects [40]. In particular, PCs containing fluid scatterers in a solid matrix [16], which can be printed on-demand and reconfigured, can be good candidates for tunable waveguiding and sensing applications. Fluid-solid coupling dynamics has become a rather extensive subject. Jin et al. [18] numerically tuned the additional localized compressional and solid–liquid coupling modes either by varying the inner radius of the pillars or controlling the height of the liquid. Amoudache et al. [41] theoretically investigated the potentiality of dual PCs for liquid sensing applications by studying the transmission through a two-dimensional (2D) crystal made of infinite cylindrical holes in a silicon substrate. However, the studies above are based on numerical simulations and remain to be experimentally verified.

In this paper, we consider a reconfigurable two-dimensional phononic metaplate inside which phononic waveguides are printed by selective fluid filling. We fabricate an epoxy sample consisting of a periodic sequence of cups attached to a plate perforated with a periodic array of cross holes and image the propagation of Lamb waves along the metaplate. The PC slab of cross holes provides us with wide band gaps. Reconfigurability and reusability are accomplished by filling water into chosen cups. Phononic band gaps are actually obtained when all cups are either empty or filled with water. Linear and 90° bent waveguides are then created with either positive or negative contrast, i.e. by filling or emptying selected cups. Numerical and experimental results are generally found to agree fairly well, despite slight resonance frequency shifts. The propagation of Lamb waves is imaged along the waveguides using a scanning laser vibrometer. Conversions between bandgaps and passing bands are clearly observed due to the coupling of elastic waves in the solid and acoustic waves in the fluid. Acoustoelastic waves are effectively observed to be guided for both straight and bent waveguides.

2. Perfect PC plates

We first consider the perfect PC plate with all cups either left empty or filled with water. The unit cell is composed of a single cup grafted onto a plate that is perforated with square lattice of cross holes, as depicted in Fig. 1(a). Geometrical parameters of the unit cell used in this paper are a=5 cm, $h = 0.8a$, $b = 0.2a$, $c_1 = 0.1a$, $r_1 = 0.38a$, $r_2 = 0.33a$, and $c_2 = 0.11a$. The epoxy sample shown in Fig. 1(b) is fabricated by a 3D printing technique. The plate and the cups are manufactured at the same time.

During experiments, a Polytec PSV-500 scanning vibrometer is used to detect and image the out-of-plane displacements at the bottom surface of the epoxy plate. A periodic chirp is chosen as the source waveform. It is amplified by the power amplifier before it is applied to the sample. The amplified signal is transformed to a displacement vibration signal via a piezoelectric patch bonded on one side of the sample. The vertical displacement signal is recorded by the vibrometer at the bottom side of the sample.

Numerical simulations are conducted by using the finite element method. We need to account for the coupling of acoustic waves in the fluid and elastic waves in the solid. Independent variables are pressure p in the fluid and displacements u_i in the solid. At the free surface between water and air, the boundary condition is taken as

$$p = 0, \tag{1}$$

hence we neglect the generation of acoustic waves in air. Note that pressure p is time-harmonic at angular frequency ω, so that the static atmospheric pressure does not appear in the above boundary condition. At the free surface between solid and air, the boundary condition is taken as

$$T_{ij} n_j = 0, \tag{2}$$

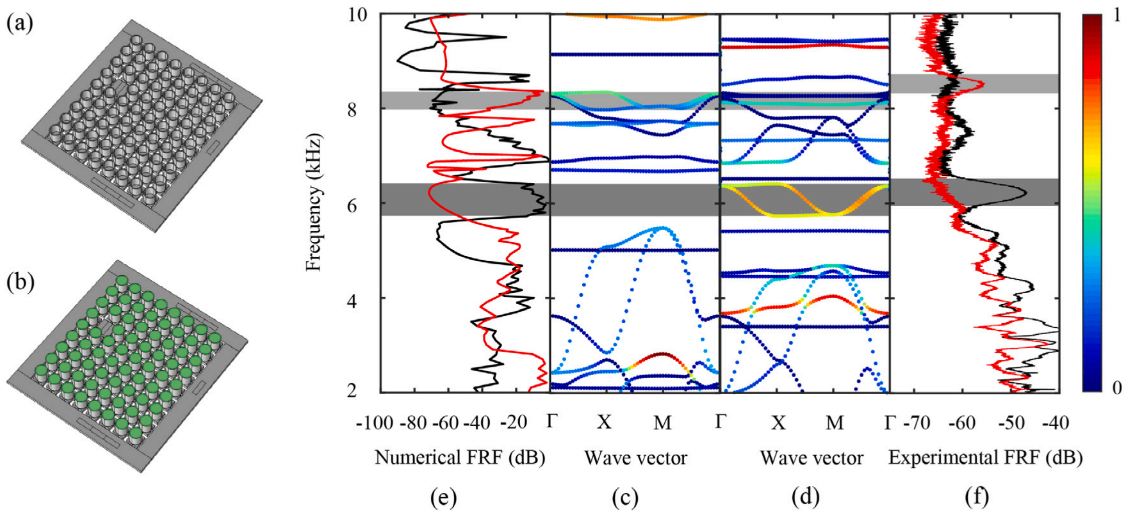

Fig. 2. Schematic representation of the solid metaplate (a) with all cups empty and (b) with all cups filled with water. The green and gray parts represent water and solid material, respectively. The phononic band structure of the perfect epoxy metaplate is shown with all cups either (c) left empty or (d) filled with water. The color scale is for the polarization amount of the out-of-plane component of displacement. Numerical (e) and experimental (f) frequency response functions (FRFs) are shown for the finite phononic metaplate with all cups either empty (red line) or filled (black line). The corresponding gray and light gray frequency ranges highlight particular bandgaps discussed in the text.

with T_{ij} the Cauchy stress tensor and where we neglect again the generation of acoustic waves in air. At the interface between solid and fluid, the boundary conditions are

$$\frac{1}{\rho_f}\frac{\partial p}{\partial n} = \omega^2 u_n, \quad T_{ij} n_j = p n_i, \tag{3}$$

where u_n is the normal displacement of the solid boundary and $\mathbf{n}$ is the normal unit vector oriented inside the fluid. These boundary conditions ensure the coupling of elastic waves in the solid and pressure acoustic waves in the fluid.

Throughout the paper, the solid material parameters for epoxy are mass density $\rho_s = 1175$ kg/m^3, Poisson's ratio $\upsilon = 0.41$, and Young's modulus $E = 3.2$ GPa; the fluid material parameters for water are mass density $\rho_f = 1000$ kg/m^3 and sound velocity $c = 1490$ m/s. Hence, the material contrast between epoxy and water is limited, since for epoxy the longitudinal velocity is 2516 m/s and the shear velocity is 983 m/s.

Considering the pressure wave equation in the fluid, the elastodynamic equation in the solid, and their coupling through the above boundary conditions, the discrete form of the acousto-elastic equations can be written [42]

$$\begin{pmatrix} \mathbf{K}_s & \mathbf{S}_{fs}^T \\ \mathbf{0} & \mathbf{K}_f \end{pmatrix}\begin{pmatrix} \mathbf{u} \\ \mathbf{p} \end{pmatrix} - \omega^2 \begin{pmatrix} \mathbf{M}_s & \mathbf{0} \\ -\mathbf{S}_{fs} & \mathbf{M}_f \end{pmatrix}\begin{pmatrix} \mathbf{u} \\ \mathbf{p} \end{pmatrix} = \begin{pmatrix} \mathbf{F} \\ 0 \end{pmatrix}, \tag{4}$$

where $\mathbf{u}$ and $\mathbf{p}$ represent respectively the displacements and the pressure at the nodes of the mesh, and $\mathbf{F}$ are nodal forces. $\mathbf{K}_s$ and $\mathbf{K}_f$ are the stiffness matrices of the solid and fluid; $\mathbf{M}_s$ and $\mathbf{M}_f$ are the mass matrices of the solid and fluid; $\mathbf{S}_{fs}$ represents the fluid-solid coupling matrix and $\mathbf{S}_{fs}^T$ is its transposed matrix. According to the dynamic equilibrium Eq. (4), we can obtain the pressure in the fluid and the displacements in the solid. For the calculation of phononic band structures, two-dimensional Bloch-Floquet periodic boundary conditions are applied at the lateral sides of the unit-cell depicted in Fig. 1(a) and there are no applied force. For the computation of the frequency response, perfectly matched layers (PMLs) are added around a mesh of the full plate to avoid reflection of elastic waves. A random wave source polarized along the z axis is applied at the position of the sample where a cup is removed. The transmitted displacements are recorded outside the crystal, on the homogeneous plate. We evaluate the frequency response by considering the ratio of the z-component of the displacements integrated over the source and the receiver. By sweeping the excitation frequency f, we evaluate the frequency response $R(f)$ in decibels units as

$$R(f) = 20\log_{10}\left(\frac{\int_{S_r} U_z \mathrm{d}s}{\int_{S_s} U_z \mathrm{d}s}\right). \tag{5}$$

S_r is the area of the receiver and S_s is the area of the source.

The phononic properties of the crystal can be considered with all cups either empty, as depicted in Fig. 2(a), or filled with water, as depicted in Fig. 2(b). The phononic band structures of the infinite and periodic crystal without water, in Fig. 2(c), and with water, in Fig. 2(d), are indeed quite different. The numerical and experimental frequency responses are further shown in Figs. 2(e) and 2(f), respectively.

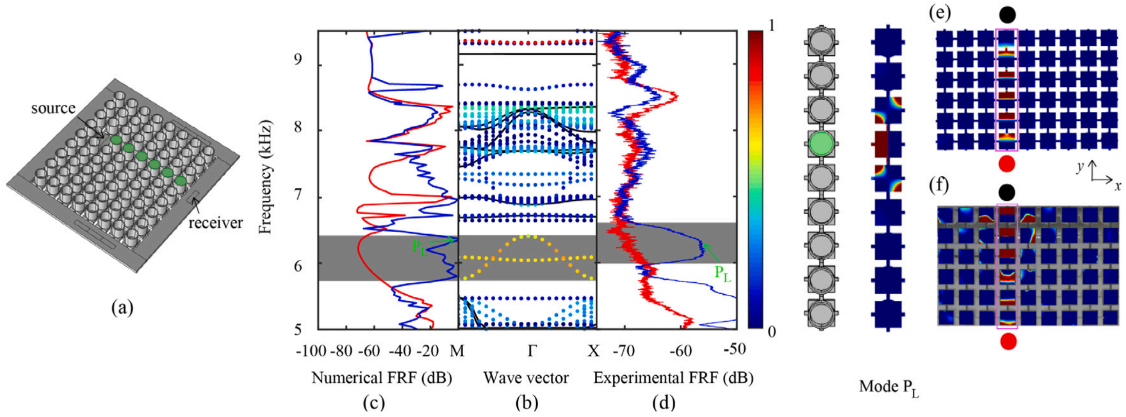

Fig. 3. Schematic representation of a positive contrast straight waveguide defined in a solid metaplate by selective filling of a line of cups (a). The green and gray parts represent water and solid material, respectively. The phononic band structure (b), and the corresponding numerical (c) and experimental (d) FRFs are presented with all cups empty (red line) or only filled along the straight waveguide (blue line). The dark-gray frequency range presents the guiding band. The calculation domain and the eigenmode P_L at the marked dispersion point are inserted. The out-of-plane displacement distribution is shown for (e) the numerical eigenmode at 6.36 kHz and (f) the experimental measurement at 6.33 kHz. The wave source and receiver positions are indicated by black and red disks, respectively. Blue (red) corresponds to zero (maximum) amplitude for the displacement field.

When water is added inside or removed from the cups, the dispersion of waves in the plate is rather strongly affected. Generally speaking, adding or removing water leads to a frequency shift of dispersion bands that is particular to each band. As a result, exchanges between certain bandgaps and passing bands are observed. In those frequency ranges, band gap engineering becomes available.

The local-resonance mechanism is not the only cause of the frequency shift of passing bands and bandgaps [16]. Owing to the fluid-solid boundary condition inside the cup and hence to acoustoelastic coupling, Lamb waves in the solid metaplate are partly converted to pressure waves in water. Furthermore, the finite and bounded volume of water leads to pressure acoustic waves decomposing onto the available modes at the particular frequency of excitation. Back conversion to Lamb waves in the solid occurs with a delay, causing an apparent slowing down of the propagation of Lamb waves along the metaplate, since the conversion is not resonant for most frequencies. As a whole, the dispersion of propagating Lamb waves is shifted down in frequency for a given wavenumber since the phase velocity is reduced. Removing water from the solid cups has the opposite effect.

In order to check the influence of energy loss on the results, the viscosity of water and the viscoelasticity of epoxy were considered as the main sources of damping. It has been argued that damping has a limited influence on transmission for large lattice constants and hence low frequencies [40]. After damping was added to the transmission model, it was indeed found that the numerical frequency response function did not change appreciably, showing only a slight difference in the frequency position of passing frequency ranges. This effect can be explained by the small group velocity of passing bands that leads to enhanced spatial decay on propagation [6]. Overall, the numerical results agree fairly well with the experimental ones when neglecting the viscosity of solid and fluid.

In the following, we consider the realization of PC waveguides defined by either positive contrast (defects are filled cups) or by negative contrast (defects are empty cups). In either case, we need a phononic band gap for the supporting crystal. Two interesting frequency ranges are highlighted in Fig. 2. Around 6.36 kHz, there is a complete band gap for empty cups, whereas around 8.35 kHz there is a full band gap for out-of-plane waves for filled cups. The central frequencies indicated are the experimental response maxima. Experimental results are globally consistent with numerical responses, except for slight frequency shifts that can possibly be attributed to the slightly inaccurate modeling of the sample, inaccurate material properties, evaporation of water during experiments, and the neglection of certain aspects of acoustoelastic coupling.

3. Straight waveguides

The observations of the previous section allow us for the design of reconfigurable waveguides and circuits with either positive or negative contrast. In the first case, waveguides operating around 6.36 kHz can be written by filling cups with water in an initially empty metaplate (positive contrast waveguides, see Fig. 3(a)). Conversely, waveguides operating around 8.35 kHz can be written by emptying cups in an initially fully filled metaplate (negative contrast waveguides, see Fig. 4(a)). We explore this idea for straight waveguides in this section.

First, phononic band structures for positive and negative contrast straight waveguides are shown in Figs. 3 and 4, respectively, together with the numerical and measured frequency responses for the finite sample. It can be clearly observed in Fig. 3(b) that additional bands appear inside the dark-gray frequency range between 5.73 kHz to 6.41 kHz after water is added into the cups defining the positive contrast straight waveguide. In contrast, additional bands appear inside the light-gray frequency range between 8.0 kHz and 8.35 kHz for negative contrast, as shown in Fig. 4(b). These guiding frequency ranges are almost the same as for the

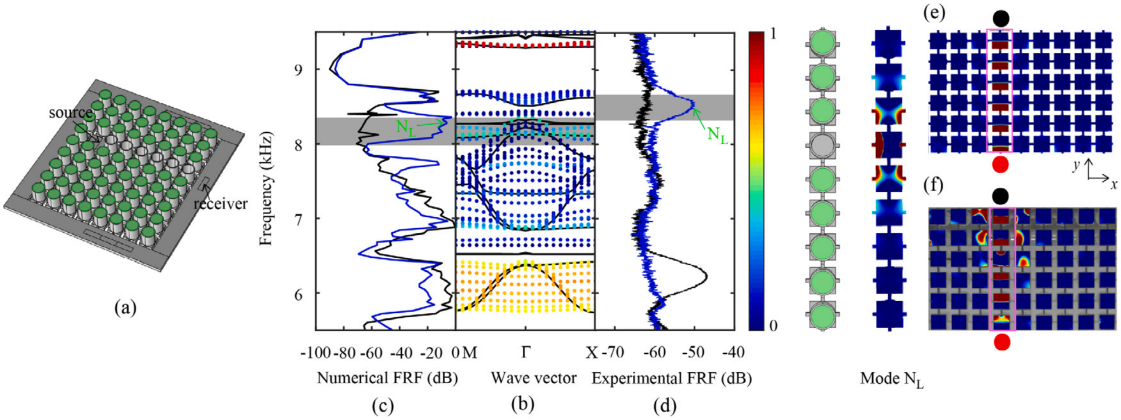

Fig. 4. Schematic representation of a negative contrast straight waveguide defined in a solid metaplate by selective emptying of a line of cups (a). The green and gray parts represent water and solid material, respectively. The phononic band structure (b), and the corresponding numerical (c) and experimental (d) FRFs are presented with all cups filled (black line) or only emptied along the straight waveguide (blue line). The dark-gray frequency range presents the guiding band. The calculation domain and the eigenmode N_L at the marked dispersion point are inserted. The out-of-plane displacement distribution is shown for (e) the numerical eigenmode at 8.35 kHz and (f) the experimental measurement at 8.47 kHz. The wave source and receiver positions are indicated by black and red disks, respectively. Blue (red) corresponds to zero (maximum) amplitude for the displacement field.

perfect PCs with all empty or filled cups. As in the case of the perfect crystal, there is a slight frequency shift between numerical simulation and experiment that may be explained similarly.

Defect eigenmodes at points P_L and N_L are shown in Figs. 3 and 4, respectively. For both eigenmodes the dipolar wave vibration is symmetric with respect to the direction of wave propagation. In both case, the vibration converts to a rotating mode in the cups adjacent to the defect cup. Rotation occurs in opposite directions on either side of the defect.

Figs. 3 and 4 also present the numerical (e) and experimental (f) distribution of the out-of-plane displacement at 6.36 kHz and 6.33 kHz for the positive contrast straight waveguide and at 8.35 kHz and 8.47 kHz for the negative contrast straight waveguide. Corresponding animations during one period of oscillation are provided in Supplementary Material [43]. The results clearly show that wave propagation is strongly confined to the defect waveguides in both case. Overall, acoustoelastic waves are effectively guided along both positive and negative straight waveguides. Reconfigurability is thus verified in the fluid-filled phononic metaplate with straight waveguides.

In order to quantify the field localization in the waveguides, a confinement degree is proposed next. Generally speaking, the confinement degree is related to the slope of the guided waves in the band structure. Guided waves are highly localized in the waveguide if the band is flat. To quantitatively evaluate the confinement in the waveguides, a concentration degree [44] of the guided wave is defined as follows:

$$C_x = \left(\frac{1}{l_y} \int \frac{1}{l_x} \int \left[\frac{|w|}{|w|_{max}} |x|^2 \right] \mathrm{d}x\mathrm{d}y \right)^{-1} \tag{6}$$

where l_x and l_y are the lengths for one row of the finite structure in the x and the y directions. $|x|$ is the distance to the excitation. The confinement degrees calculated for positive and negative contrast waveguides are $C_x = 25.13$ m^{-2} and $C_x = 26.06$ m^{-2}, respectively. There is only a slight difference between both contrasts.

4. Bent waveguides

In this section, we turn our attention to bent waveguides. Waveguides with one 90° bend, as shown in Figs. 5(a) and 6(a), are defined by either positive or negative contrast. In this case, the waveguide is not periodic and computing a phononic band structure is not adequate. In contrast, the frequency response can still be obtained and compared to experimental results. In the numerical and experimental frequency responses shown in Figs. 5 and 6, it is apparent that excitation of the waveguide beyond the bend can be obtained again around 6.3 kHz and 8.3 kHz, in accordance with the largest portion of the transmission bandwidths observed for the straight waveguides and the bare PC. A fair agreement is obtained between numerical and experimental results, though some differences exist.

Figs. 5 and 6 also present the numerical and experimental field distribution of the out-of-plane displacement at 6.36 kHz and 6.38 kHz, respectively, for positive contrast (8.35 kHz and 8.41 kHz for negative contrast, respectively). The vibration is mainly localized along the defect waveguide. In the waveguide section before the bend, vibrations of the defective unit cells are symmetric with respect to the direction of propagation, similarly to the case of straight waveguides. After the bend, however, symmetry with respect to the direction of propagation is lost. Vibrations seem to be a superposition of two orthogonal dipolar components, oriented along the x and the y axes, and effectively inducing an elliptical vibration. This effect can especially be observed in the animations shown in Supplementary Material [43].

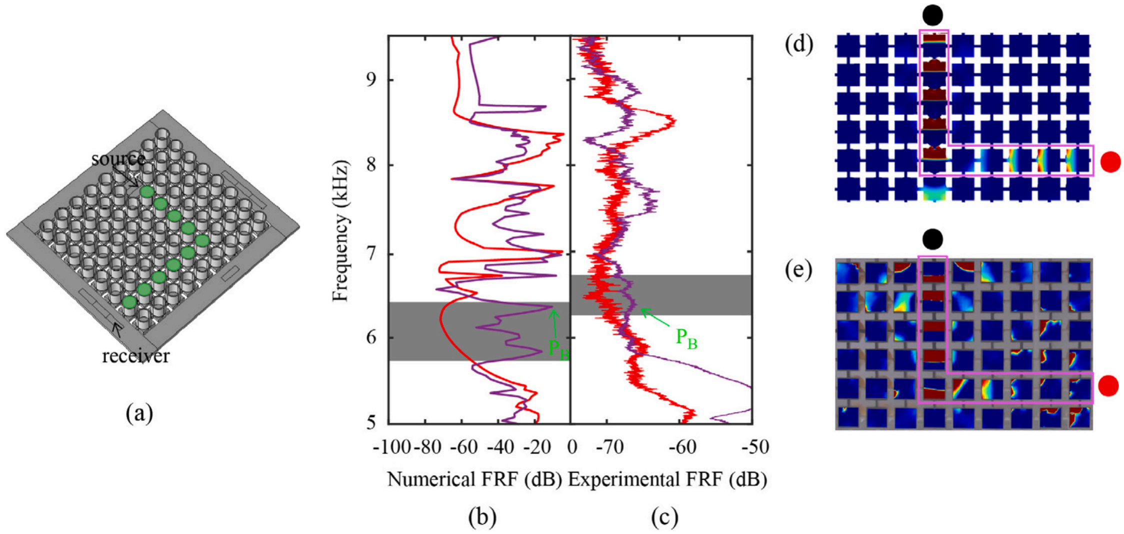

Fig. 5. Schematic representation of a positive contrast bent waveguide defined in a solid metaplate by selective filling of a line of cups (a). The green and gray parts represent water and solid material, respectively. The numerical (b) and experimental (c) FRFs are presented with all cups empty (red line) or only filled along the waveguide (purple line). The dark-gray frequency range presents the guiding band. The out-of-plane displacement distribution is shown for (d) the numerical response at 6.36 kHz and (e) the experimental measurement at 6.38 kHz. The wave source and receiver positions are indicated by black and red disks, respectively. Blue (red) corresponds to zero (maximum) amplitude for the displacement field.

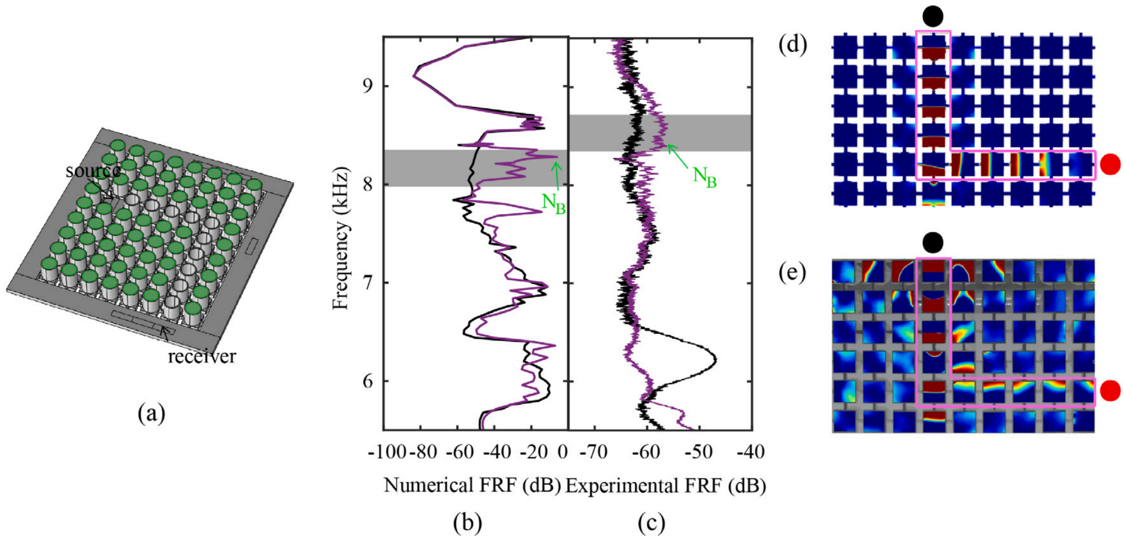

Fig. 6. Schematic representation of a negative contrast bent waveguide defined in a solid metaplate by selective emptying of a line of cups (a). The green and gray parts represent water and solid material, respectively. The numerical (b) and experimental (c) FRFs are presented with all cups filled (black line) or only emptied along the straight waveguide (purple line). The light-gray frequency range presents the guiding band. The out-of-plane displacement distribution is shown for (e) the numerical eigenmode at 8.35 kHz and (f) the experimental measurement at 8.41 kHz. The wave source and receiver positions are indicated by black and red disks, respectively. Blue (red) corresponds to zero (maximum) amplitude for the displacement field.

5. Conclusions

In this paper, we have demonstrated experimentally how a phononic metaplate of cups on a cross-like PC slab can be reconfigured to create waveguides on demand by filling selected cups or emptying them. The square lattice epoxy phononic metaplate is 3D printed and is completely reusable. The crystal possesses band gaps when the cups are either all empty or all filled with water. Creating defects by either filling or emptying selected cups then allows one to implement phononic waveguides or circuits with either positive or negative contrast. The dispersion of the coupled acoustoelastic waves in the sample is controlled through fluid-solid interaction within the solid cups. Straight and bent waveguides were formed by either positive or negative contrast. They were characterized by an imaging scanning laser vibrometer. Strongly confined wave propagation was observed in all cases. Furthermore, transmission of strongly confined waves along 90° bent waveguides was observed experimentally and conversion of linear to elliptic modal polarization at the bend was noted. Experimental results were found to be in fair agreement with numerical results in all cases.

The present work paves the way for the reconfigurable manipulation of waves in phononic metaplates through the acoustoelastic interaction. Based on the concepts exposed in this work, different acoustic circuits can be designed and realized without redesigning the supporting metaplate. They are compatible with coupled resonator acoustoelastic waveguides and arbitrary resonant circuits [45]. They could also be a basis with potential for achieving further active and smart acoustic devices. Indeed, notwithstanding the consideration of tunable solid materials, the operation of the metadevice can also be tuned through the material properties of the fluid constituent, through the combination of different fluid materials, by changing the temperature of the materials or by applying an external control field such as an electric or magnetic field.

CRediT authorship contribution statement

Ting-Ting Wang: Conceptualization, Software, Investigation, Validation, Writing – original draft. **Yan-Feng Wang:** Conceptualization, Funding acquisition, Project administration, Writing – review & editing. **Zi-Chen Deng:** Validation, Writing – review & editing. **Vincent Laude:** Methodology, Project administration, Writing – review & editing. **Yue-Sheng Wang:** Validation, Funding acquisition, Project administration.

Acknowledgments

The authors acknowledge financial support by the National Natural Science Foundation of China (12102350, 12122207, and 12021002). Y.F.W. acknowledges support by the Natural Science Foundation of Tianjin, China (20JCQNJC01030). V.L. acknowledges financial support by the EIPHI Graduate School (ANR-17-EURE-0002).

Appendix A. Supplementary data

Supplementary material related to this article can be found online at https://doi.org/10.1016/j.ymssp.2021.108392.

References

[1] E. Yablonovitch, Inhibited spontaneous emission in solid-state physics and electronics, Phys. Rev. Lett. 58 (20) (1987) 2059.
[2] M.S. Kushwaha, P. Halevi, L. Dobrzynski, B. Djafari-Rouhani, Acoustic band structure of periodic elastic composites, Phys. Rev. Lett. 71 (13) (1993) 2022.
[3] J. Vasseur, B. Djafari-Rouhani, L. Dobrzynski, M. Kushwaha, P. Halevi, Complete acoustic band gaps in periodic fibre reinforced composite materials: the carbon/epoxy composite and some metallic systems, J. Phys.: Condens. Matter 6 (42) (1994) 8759.
[4] C.-S. Kee, J.-E. Kim, H.Y. Park, K.-J. Chang, H. Lim, Essential role of impedance in the formation of acoustic band gaps, J. Appl. Phys. 87 (4) (2000) 1593–1596.
[5] M.I. Hussein, M.J. Frazier, Band structure of phononic crystals with general damping, J. Appl. Phys. 108 (9) (2010) 093506.
[6] R.P. Moiseyenko, V. Laude, Material loss influence on the complex band structure and group velocity in phononic crystals, Phys. Rev. B 83 (6) (2011) 064301.
[7] B. Merheb, P.A. Deymier, K. Muralidharan, J. Bucay, M. Jain, M. Aloshyna-Lesuffleur, R. Greger, S. Mohanty, A. Berker, Viscoelastic effect on acoustic band gaps in polymer-fluid composites, Modelling Simulation Mater. Sci. Eng. 17 (7) (2009) 075013.
[8] M.J. Frazier, M.I. Hussein, Viscous-to-viscoelastic transition in phononic crystal and metamaterial band structures, J. Acoust. Soc. Am. 138 (5) (2015) 3169–3180.
[9] M.J. Frazier, M.I. Hussein, Generalized Bloch's theorem for viscous metamaterials: Dispersion and effective properties based on frequencies and wavenumbers that are simultaneously complex, Comptes Rendus Physique 17 (5) (2016) 565–577.
[10] M. Gei, S. Roccabianca, M. Bacca, Controlling bandgap in electroactive polymer-based structures, IEEE/ASME Trans. Mechatronics 16 (1) (2010) 102–107.
[11] F. Nazari, J. Babaki, Heterostructure based demultiplexer using solid-solid phononic crystal ring resonators, J. Phys. D: Appl. Phys. (2020).
[12] A.H. Aly, A. Nagaty, Z. Khalifa, A. Mehaney, The significance of temperature dependence on the piezoelectric energy harvesting by using a phononic crystal, J. Appl. Phys. 123 (18) (2018) 185102.
[13] A.H. Aly, A. Nagaty, A. Mehaney, Thermal properties of one-dimensional piezoelectric phononic crystal, Eur. Phys. J. B 91 (10) (2018) 1–5.
[14] M.J. Leamy, Exact wave-based Bloch analysis procedure for investigating wave propagation in two-dimensional periodic lattices, J. Sound Vib. 331 (7) (2012) 1580–1596.
[15] A.H. Safavi-Naeini, O. Painter, Design of optomechanical cavities and waveguides on a simultaneous bandgap phononic-photonic crystal slab, Opt. Express 18 (14) (2010) 14926–14943.
[16] T.-T. Wang, Y.-F. Wang, Y.-S. Wang, V. Laude, Tunable fluid-filled phononic metastrip, Appl. Phys. Lett. 111 (4) (2017) 041906.
[17] Y. Pennec, B. Djafari-Rouhani, H. Larabi, J. Vasseur, A.-C. Hladky-Hennion, Phononic crystals and manipulation of sound, Phys. Status Solidi C 6 (9) (2009) 2080–2085.
[18] Y. Jin, Y. Pennec, Y. Pan, B. Djafari-Rouhani, Phononic crystal plate with hollow pillars actively controlled by fluid filling, Crystals 6 (6) (2016) 64.
[19] N. Laforge, V. Laude, F. Chollet, A. Khelif, M. Kadic, Y. Guo, R. Fleury, Observation of topological gravity-capillary waves in a water wave crystal, New J. Phys. 21 (8) (2019) 083031.
[20] R. Anufriev, M. Nomura, Heat conduction engineering in pillar-based phononic crystals, Phys. Rev. B 95 (15) (2017) 155432.
[21] E.A.F. Parra, A. Bergamini, L. Kamm, P. Zbinden, P. Ermanni, Implementation of integrated 1D hybrid phononic crystal through miniaturized programmable virtual inductances, Smart Mater. Struct. 26 (6) (2017) 067001.
[22] Y. Zhang, B. Li, Q. Zheng, G.M. Genin, C. Chen, Programmable and robust static topological solitons in mechanical metamaterials, Nature Commun. 10 (1) (2019) 1–8.
[23] A.M. Ahmed, A. Mehaney, M. Shaban, A.H. Aly, Scattering spectra of magneto-plasmonic core/shell nanoparticle based on mie theory, Mater. Res. Express 6 (8) (2019) 085073.
[24] B. Florijn, C. Coulais, M. van Hecke, Programmable mechanical metamaterials, Phys. Rev. Lett. 113 (17) (2014) 175503.

[25] Y. Pennec, B. Djafari-Rouhani, J. Vasseur, A. Khelif, P.A. Deymier, Tunable filtering and demultiplexing in phononic crystals with hollow cylinders, Phys. Rev. E 69 (4) (2004) 046608.
[26] Y.-F. Wang, Y.-Z. Wang, B. Wu, W. Chen, Y.-S. Wang, Tunable and active phononic crystals and metamaterials, Appl. Mech. Rev. 72 (4) (2020) 040801.
[27] M.R. Singh, J. Guo, J.M. Cid, P.C. Sharma, A.H. Aly, B. Bhadoria, J.E. De Hoyos Martinez, Phonon conductivity of nanoparticles embedded in dielectric material, Phys. Status Solidi B 255 (8) (2018) 1700681.
[28] A.H. Aly, S.M. Shaban, A. Mehaney, High-performance phoxonic cavity designs for enhanced acousto-optical interaction, Appl. Opt. 60 (11) (2021) 3224–3231.
[29] A. Rostami, H. Kaatuzian, B. Rostami-Dogolsara, Acoustic 1× 2 demultiplexer based on fluid-fluid phononic crystal ring resonators, J. Molecular Liquids 308 (2020) 113144.
[30] A. Nagaty, A. Mehaney, A.H. Aly, Acoustic wave sensor based on piezomagnetic phononic crystal, J. Supercond. Nov. Magn. 31 (12) (2018) 4173–4177.
[31] S.M. Shaban, A. Mehaney, A.H. Aly, Determination of 1-propanol, ethanol, and methanol concentrations in water based on a one-dimensional phoxonic crystal sensor, Appl. Opt. 59 (13) (2020) 3878–3885.
[32] A.H. Aly, A. Nagaty, A. Mehaney, One-dimensional phononic crystals that incorporate a defective piezoelectric/piezomagnetic as a new sensor, Eur. Phys. J. B 91 (10) (2018) 1–5.
[33] S.E. Zaki, A. Mehaney, H.M. Hassanein, A.H. Aly, High-performance liquid sensor based one-dimensional phononic crystal with demultiplexing capability, Mater. Today Commun. 26 (2021) 102045.
[34] S.E. Zaki, A. Mehaney, H.M. Hassanein, A.H. Aly, Fano resonance based defected 1D phononic crystal for highly sensitive gas sensing applications, Sci. Rep. 10 (1) (2020) 1–16.
[35] H. Zhu, F. Semperlotti, Metamaterial based embedded acoustic filters for structural applications, AIP Adv. 3 (9) (2013) 092121.
[36] M. Ghasemi Baboly, C.M. Reinke, B.A. Griffin, I. El-Kady, Z.C. Leseman, Acoustic waveguiding in a silicon carbide phononic crystals at microwave frequencies, Appl. Phys. Lett. 112 (10) (2018) 103504.
[37] Y.-F. Wang, T.-T. Wang, J.-P. Liu, Y.-S. Wang, V. Laude, Guiding and splitting Lamb waves in coupled-resonator elastic waveguides, Compos. Struct. 206 (2018) 588–593.
[38] M. Ghasemi Baboly, A. Raza, J. Brady, C.M. Reinke, Z.C. Leseman, I. El-Kady, Demonstration of acoustic waveguiding and tight bending in phononic crystals, Appl. Phys. Lett. 109 (18) (2016) 183504.
[39] T.-T. Wang, Y.-F. Wang, Y.-S. Wang, V. Laude, Evanescent-wave tuning of a locally resonant sonic crystal, Appl. Phys. Lett. 113 (23) (2018) 231901.
[40] Y.-F. Wang, T.-T. Wang, Y.-S. Wang, V. Laude, Reconfigurable phononic-crystal circuits formed by coupled acoustoelastic resonators, Phys. Rev. A 8 (1) (2017) 014006.
[41] S. Amoudache, Y. Pennec, B. Djafari Rouhani, A. Khater, R. Lucklum, R. Tigrine, Simultaneous sensing of light and sound velocities of fluids in a two-dimensional phoXonic crystal with defects, J. Appl. Phys. 115 (13) (2014) 134503.
[42] Y.-F. Wang, S.-Y. Zhang, Y.-S. Wang, V. Laude, Hybridization of resonant modes and Bloch waves in acoustoelastic phononic crystals, Phys. Rev. B 102 (14) (2020) 144303.
[43] See Supplemental Material at [URL will be inserted by publisher] for the animation of the numerical (a) and experimental (b) z-component of the displacement distribution of the epoxy metaplate with positive and negative contrast waveguides.
[44] Y.-F. Wang, Y.-S. Wang, C. Zhang, Bandgaps and directional propagation of elastic waves in 2D square zigzag lattice structures, J. Phys. D: Appl. Phys. 47 (48) (2014) 485102.
[45] T.-T. Wang, S. Bargiel, F. Lardet-Vieudrin, Y.-F. Wang, Y.-S. Wang, V. Laude, Collective resonances of a chain of coupled phononic microresonators, Phys. Rev. A 13 (1) (2020) 014022.